C. R. Mecanique 347 (2019) 615–625

Contents lists available at ScienceDirect

Comptes Rendus Mecanique

www.sciencedirect.com

Experimental and numerical study of the effect of silica filler on the tensile strength of a 3D-printed particulate nanocomposite

Muhammad Asif [a,b], Maziar Ramezani [a,*], Kamran Ahmed Khan [d], Muhammad Ali Khan [e], Kean Chin Aw [c]

[a] Department of Mechanical Engineering, Auckland University of Technology, Auckland, New Zealand
[b] Department of Engineering Sciences, National University of Science and Technology, Karachi, Pakistan
[c] Department of Mechanical Engineering, University of Auckland, Auckland, New Zealand
[d] Aerospace Engineering Department, Khalifa University, Abu Dhabi, United Arab Emirates
[e] School of Aerospace, Transport and Manufacturing, Cranfield University, UK

ARTICLE INFO

Article history:
Received 11 July 2019
Accepted 30 July 2019
Available online 3 September 2019

Keywords:
3D printing
Hyperelastic
Photopolymer extrusion
Viscoelastic

ABSTRACT

Polymers are commonly found to have low mechanical properties, e.g., low stiffness and low strength. To improve the mechanical properties of polymers, various types of fillers have been added. These fillers can be either micro- or nano-sized; however; nano-sized fillers are found to be more efficient in improving the mechanical properties than micro-sized fillers. In this research, we have analysed the mechanical behaviour of silica reinforced nanocomposites printed by using a new 5-axis photopolymer extrusion 3D printing technique. The printer has 3 translational axes and 2 rotational axes, which enables it to print free-standing objects. Since this is a new technique and in order to characterise the mechanical properties of the nanocomposites manufactured using this new technique, we carried out experimental and numerical analyses. We added a nano-sized silica filler to enhance the properties of a 3D printed photopolymer. Different concentrations of the filler were added and their effects on mechanical properties were studied by conducting uniaxial tensile tests. We observed an improvement in mechanical properties following the addition of the nano-sized filler. In order to observe the tensile strength, dog-bone samples using a new photopolymer extrusion printing technique were prepared. A viscoelastic model was developed and stress relaxation tests were conducted on the photopolymer in order to calibrate the viscoelastic parameters. The developed computational model of nano reinforced polymer composite takes into account the nanostructure and the dispersion of the nanoparticles. Hyper and viscoelastic phenomena was considered to validate and analyse the stress–strain relationship in the cases of filler concentrations of 8%, 9%, and 10%. In order to represent the nanostructure, a 3D representative volume element (RVE) was utilized and subsequent simulations were run in the commercial finite element package ABAQUS. The results acquired in this study could lead to a better understanding of the mechanical characteristics of the nanoparticle

* Corresponding author.
E-mail address: maziar.ramezani@aut.ac.nz (M. Ramezani).

https://doi.org/10.1016/j.crme.2019.07.003
1631-0721/© 2019 Académie des sciences. Published by Elsevier Masson SAS. All rights reserved.

reinforced composite, manufactured using a new photopolymer extrusion 5-axis 3D printing technique.

© 2019 Académie des sciences. Published by Elsevier Masson SAS. All rights reserved.

1. Introduction

The most common technique to enhance the properties of polymers consists in adding reinforcements, for example, nanoparticles or fibres. Several composites have been manufactured by adding micro sized reinforcements in the past twenty years [1–3]. In the past two decades, nano-sized reinforcements have attracted a significant interest from the scientific and industrial sectors. In fact, the nano-sized reinforced composites have proven to show better mechanical behaviour when compared with conventional ones [4,5]. Especially, a significant amount of interest has been dedicated to bi-phase or multiphase systems in which inorganic nano fillers are added to the polymer. These nanometric fillers produce large surface area if homogenously distributed in the matrix; thus, these systems can potentially enhance the interfacial interaction between matrix and filler, resulting in improved mechanical properties of the material [6]. Researchers have reported a considerable amount of enhancement in mechanical and tribological properties, even at very low volume fractions [7]. Especially, some researchers have reported that ceramic and nano-sized silica particles can prominently enhance the bulk mechanical properties of polymers [7–9].

Finite Element Modelling (FEM) has been successfully implemented by some researchers to model the composites being reinforced with nanometric fillers. For instance, Liu and Chen [10] studied the possibility of applying FEM to composites reinforced with carbon nanotube using representative volume element (RVE). Other numerical techniques such as 3D FEM and 2D nano scale FEM were also used by other researchers to model the mechanical behaviour of nanocomposite materials [11–13]. It can be noted that such FEM based models are commonly executed by using representative volume elements, thus making the assumption that the nanocomposite microstructure can be replicated by gathering large quantities of these elements. An RVE normally has one or more nanofiller(s) that are surrounded by a resin, and adequate loads or boundary conditions are applied to predict the effect of the surrounding materials. It is considered as a building block to accumulate the composite. Until now, a majority of the studies focused on the linear elastic properties and yielding predictions for the elastic toughness of the nanocomposites with respect to filler concentration, filler properties, and in some cases filler orientation.

Zhang et al. [14] utilized the RVE technique to analyse the mechanical behaviour, with particular attention to the damage mechanisms of SiCp-reinforced Al composites using experiments and FEM. They developed a 3D microstructure FEM model predicting the elastoplastic behaviour and the breakage behaviour of a 7% volume fraction of SiCp-reinforced Al composite. Hua et al. [15] studied the mechanical behaviour of the dental composite resin reinforced with titanium oxide nanoparticles using a 3D nanoscale RVE. They characterised the effect of the nano filler concentration, geometrical aspect, toughness and interphase zone among the matrix material and the nano-filler on the bulk properties of the composite. Hua et al. [16] used nanoscale RVE to study the interphase properties and the geometry effect on the mechanical behaviour of the silica–epoxy resin nanocomposite. They found that interphase modulus and interfacial bonding conditions have a notable effect on the effective stiffness of nanocomposites.

Three-dimension (3D) printing, commonly known as additive manufacturing, follows the principle of laying down successive layers of material (sheet material, powder, or liquid) on top of each other by detecting the data from CAD file [17,18]. There are different 3D printers that are used to manufacture polymers, e.g., stereolithography (SLA), fused deposition modelling (FDM), UV assisted 3D-printing (UV3DP), etc. Micro- and nano-fillers are added to enhance the properties of the polymers manufactured using these techniques. We have developed a novel photopolymer extrusion (PPE) 3D-printing technique that uses 5 axes and is the combination of the UV3DP and FDM techniques. This technique has 3 translational axes and 2 rotational axes. Photopolymer extrusion combined with 2 rotational axes on the extrusion unit provides the possibility of printing complex free forms and free standing structures more easily. A peristaltic pump is used to accurately handle the quantity of material deposited. As discussed above, polymers exhibit weak mechanical properties, so we have added a silica nano-filler to enhance the mechanical properties of the nanocomposites manufactured using this technique. As this is a relatively new technique, there is a need for conducting experimental and numerical analyses to explore the mechanical strength and viscoelasticity of the nanocomposites printed.

A nanoscale RVE is used to predict the mechanical behaviour of fumed silica-reinforced 3D printed particulate nanocomposite, different concentrations of the filler were added, and dog bone samples were printed. Stress relaxation tests were conducted on the polymer to characterise the viscoelastic properties, and tensile tests were conducted on each concentration to observe the tensile strength and strain to failure. The multi-scale material modelling platform DIGIMAT [19] was used to develop the RVE to represent the nanostructure of the composite; subsequent simulations were conducted in the commercial finite-element software ABAQUS to validate the behaviour of the nanocomposite after importing the user defined python script as input.

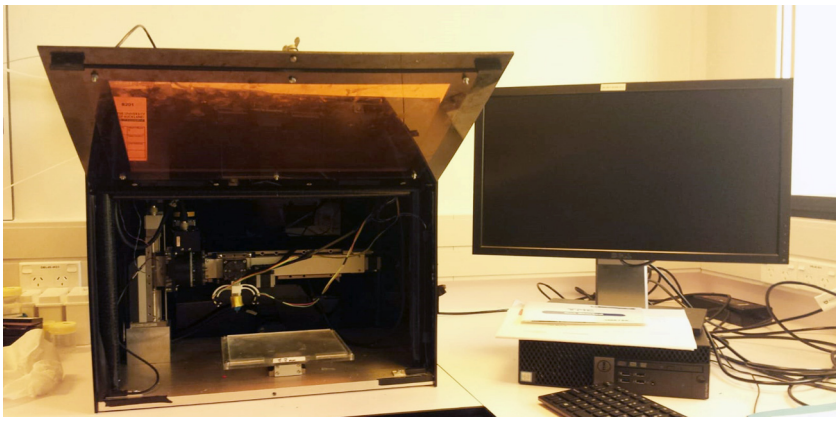

Fig. 1. Schematic of the 5-axis photopolymer extrusion printer.

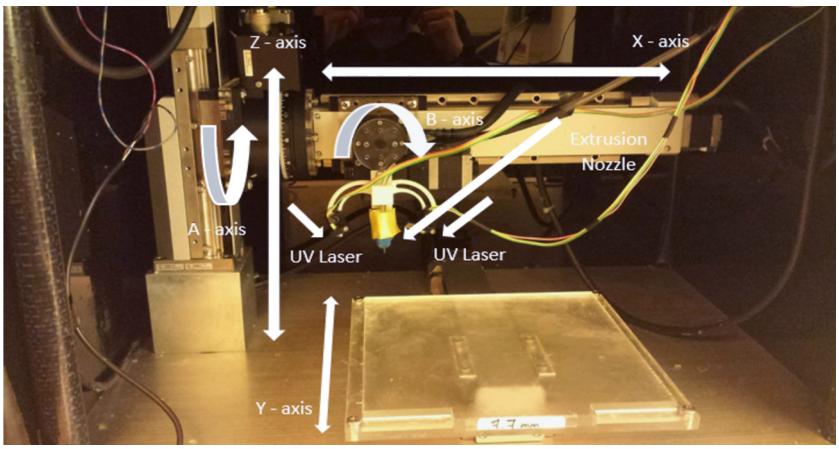

Fig. 2. Close up view of the 5-axis PPE printer.

2. Experimental procedure

2.1. Photopolymer extrusion (PPE) 3D printer

Fig. 1 shows the novel (PPE) 5-axis 3D printing machine. Fig. 2 shows a close-up view of the new printer outlining the 5 axes and extrusion unit with 2 UV lasers on either side. The whole PPE 5-axes system consists of two UV laser diodes used to cure the photopolymer, a peristaltic pump and a nozzle that serves as an extrusion system and a platform consisting of conventional axes (X, Y, and Z) along with two rotational axes (A and B).

This PPE 5-axis 3D printer has an FDM-style extrusion system. An extruder unit is used to deposit the photopolymer resin. UV lasers mounted on each side of the printing nozzle cure the photopolymer soon after it leaves the nozzle [20].

2.2. Composition of photopolymer resin

The photopolymer resin used in this study (UV Dome 58) was supplied by Whitehall Technical Services Ltd, Auckland, New Zealand. It is an epoxy urethane in which fumed silica was utilized as a filler. As depicted in Fig. 3, the filler used has a spherical shape having an approximate size between 25 to 30 nm. Fumed silica particles have the tendency to form agglomeration. The size of the agglomerates increases with increasing particle loading. The photopolymer resin is curable with UV exposure at a wavelength of 405 nm.

In order to investigate the effect of the filler on the tensile strength of printed parts, specimens with varying concentrations of fumed silica (by weight) were composed by mixing it into the photopolymer. In order for the specimens to have same ageing, blends were composed the same day and the entire blend composition process was carried out inside a photolithography room. An amount of 100 g of blend was prepared for every concentration, for example for 4% by weight of filler, 96 g of the photopolymer were mixed with 4 g of fumed silica filler. A thin spatula was used to manually stir the mixture for 5–10 minutes; after this, the blend was mixed with an ultrasonic homogeniser. An ultrasonic homogeniser from

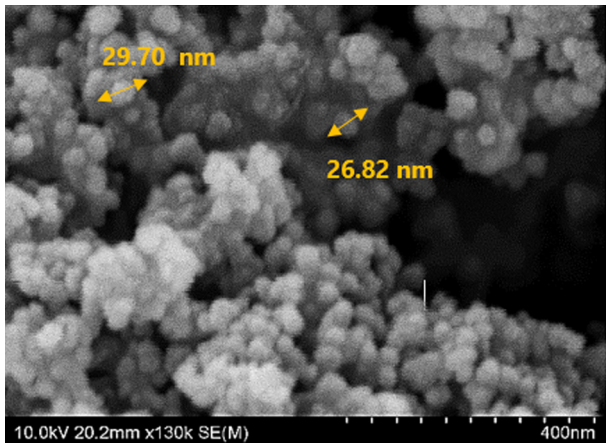

Fig. 3. SEM of the silica nanoparticles.

Table 1
Dynamic viscosity versus filler concentration.

S. No	Filler concentration (%)	Viscosity (cP)
1	0	6048
2	2	7545
3	4	8289
4	6	9960
5	8	14 860
6	9	16 900
7	10	25 000
8	11	35 700
9	12	79 800

Sonics and Materials Inc [21] was used for 2 min at an ultrasound frequency of 20 kHz and an intensity of 130 W. In the end, to reduce air bubbles, specimens were vacuumed for 45 min at 65 °C.

2.3. Adequate material viscosity for printing

For well-ordered extrusion, the viscosity of the material has to be in an adequate range. Low viscosity is likely to cause the material to expand due to gravitational factor prior to the curing by the UV laser, high viscosity causes difficulties in depositing the material through the extruder unit. Therefore, the viscosities of the photopolymer blends were carefully calculated as a function of the filler concentrations mentioned in Table 1 using a rheometer, and their capability to print reliably was observed. In order to accurately measure the viscosity of the resin with the concentrations used, a 64-gauge spindle was used. For each sample, the revolution speed was adjusted to achieve a torque close to the midpoint (50%) of the sensor range. The rheometer then calculated the viscosity value based on the spindle, speed, and the measured torque.

As depicted in Table 1, substantial growth in the dynamic viscosity is detected with respect to the increase in the proportion of filler. Filler concentrations up to 6% have low viscosity and an abrupt increase in viscosity was seen with filler concentrations higher than 9%. A small scale of filler concentrations of 8%, 9% and 10% (compatible with dynamic viscosities from of 15 000 cP to 25 000 cP) with the extrusion nozzle of 21 gauge (0.5 mm) was found to be the appropriate range to obtain smooth printing.

2.4. Tensile test

In order to observe the tensile strength of the parts printed, dog-bone specimens according to ASTM D638 standard type V (Fig. 4) were printed (Fig. 5) and tensile tests were conducted on each specimen to observe the tensile strength and strain to failure. Table 2 shows the process parameters used to print the samples, including the values used for layer heights and printing speed. Table 3 shows the mechanical properties of 8%, 9% and 10% filler concentrations. Each test set has been repeated three times and the average values are reported in Table 3.

As discussed in section 1, fillers are employed to enhance the mechanical properties of the polymers. However, there are certain characteristics on which the overall strength of the nanocomposite rely, e.g., matrix–particle interfacial adhesion, particle size, and particle loading [22]. Whereas it is generally accepted that adding fillers might increase the mechanical properties of the nanocomposite, stresses sometimes do not behave as expected [23]. Particle size plays a very important

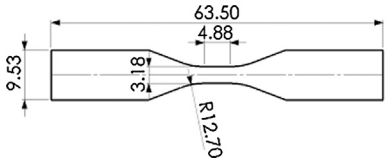

Fig. 4. ASTM (D638) type V dog-bone specimen.

Fig. 5. ASTM D638 and printed specimen.

Table 2
Process parameters used to print the samples.

Process parameters	Variables		
Print setting	Layers and perimeters	Layer height (mm) First layer height (mm)	3.22 0.20
	Infill	Fill density (%)	40
	Speed (print moves)	Perimeters (mm/s) Infill (mm/s)	20 40
	Overall time/sample	(min)	10
Filament setting	Filament	Diameter (mm)	1
	Extrusion	Extrusion multiplier	0.0055

Table 3
Mechanical properties of 8%, 9% and 10% filler concentrations.

Filler concentration (%)	Tensile strength (MPa)	Strain at break (%)
8%	28	11
9%	22.2	5.6
10%	23.6	8.6

role in increasing the strength of the composite. Dittanet and Pearson [23] studied the effects of different particle sizes on the composites tensile strength by increasing the volume fraction, and concluded that nano-sized particles increase the tensile strength with increasing volume fraction. This is true as smaller particles have larger surface area, providing more enhanced matrix-particle interfacial adhesion, which results in effective transfer of the stress from the matrix to particles. Increasing the filler content increases the diameter of the filler and thereby decreases the surface area, which sometimes results in poor matrix–particle interfacial adhesion, and, as a result, the nanoparticles cannot withstand a majority of the externally applied force. Therefore, the mechanical properties of the composite will be similar as that of neat resin.

As shown in Table 3, the tensile strength of a sample with a filler concentration of 8% is higher than that of samples with concentrations of 9% and 10%; this is due to better interfacial adhesion, because at a lower filler concentration nanoparticles have a larger surface area, which gives rise to a better bonding between the matrix and the nanoparticles. The tensile strength of a sample with a filler concentration of 10% is close to that of a sample with a filler concentration of 9%, but is lower than that of a sample with a filler concentration of 8%, because a higher filler content increases the diameter and decreases the surface area, which results in weak interfacial adhesion, leading to weak mechanical properties. Fig. 6 shows the stress–strain curves of samples with filler concentrations of 8%, 9%, and 10%; it can be seen that increasing the volume fraction made the samples less elastic, as the strain at break of both samples (i.e. with filler concentrations of 9% and 10%) is smaller compared to that with a filler concentration of 8%.

3. Finite-element simulation procedure

3.1. Constitutive equations

The experimental stress–stain data of polymer UV Dome 58 were used to calibrate an isotropic hyperelastic strain energy density function (SEDF) in ABAQUS in order to obtain the material constants to be used in our FE simulations. After performing the curve-fitting procedure in ABAQUS, out of various SEDF available, Yeoh's function captured the behaviour of the photopolymer more accurately, as shown in Fig. 7. Yeoh's model in the form of SEDF can be written as

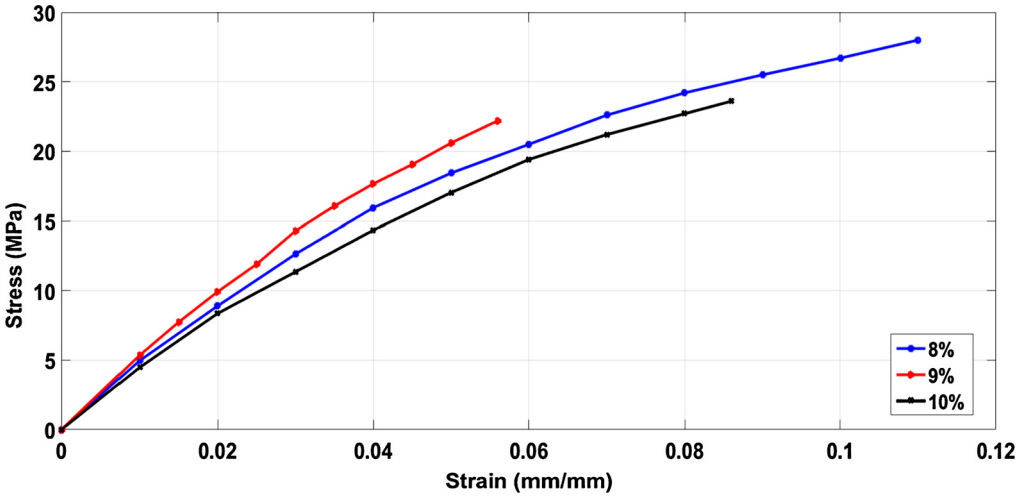

Fig. 6. Stress-strain curve for filler concentrations of 8%, 9%, and 10%.

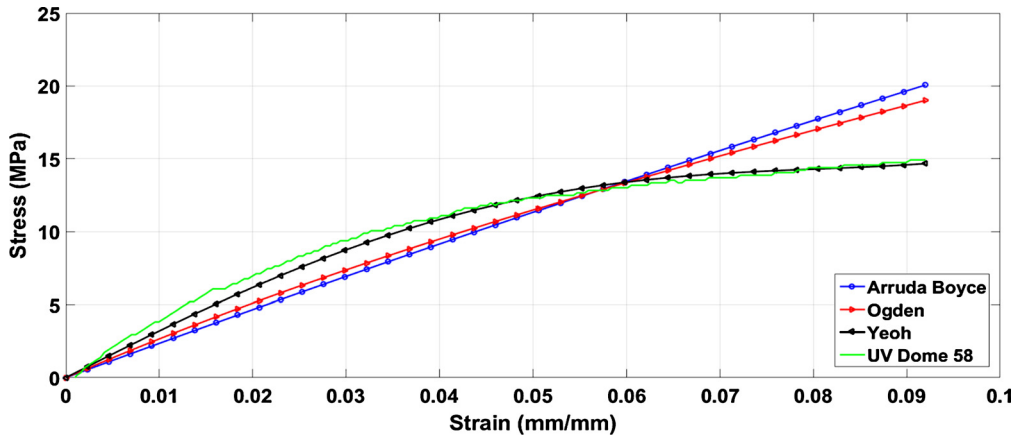

Fig. 7. Curve fitting using different SEDF in ABAQUS.

Table 4
Material constants for Yeoh's SEDF.

C_{10} (MPa)	C_{20} (MPa)	C_{30} (MPa)	D_1	D_2	D_3
76.88	−1225.40	13 201.63	6.002e-3	0	0

$$W = \sum_{i=1}^{3} C_{i0}(\bar{I}_1 - 3)^i + \sum_{i=1}^{N} \frac{1}{D_i}(J-1)^{2i} \tag{1}$$

where $J = \det(F)$ and F is considered as the deformation gradient. The term $\bar{I}_1$ is the first invariant of the left Cauchy–Green strain tensor B. ABAQUS employs linear least square fitting in order to calibrate the material constants. The calibrated material constants of the Yeoh's function are shown in Table 4.

3.2. Stress relaxation test

ABAQUS uses Prony series in order to obtain the coefficients of the viscoelastic material as shown in Eq. (2). To calibrate the Prony series coefficients in ABAQUS, a stress relaxation test was conducted at room temperature, the sample was subjected to a constant strain of 6% applied at a rate of 3 mm/min. The curve-fitting procedure was carried out as shown in Fig. 8; it is quite evident from Fig. 8 that the normalized shear moduli obtained from ABAQUS are in good agreement with the experimental stress relaxation data. Table 5 shows the Prony series coefficients obtained by the curve fitting procedure:

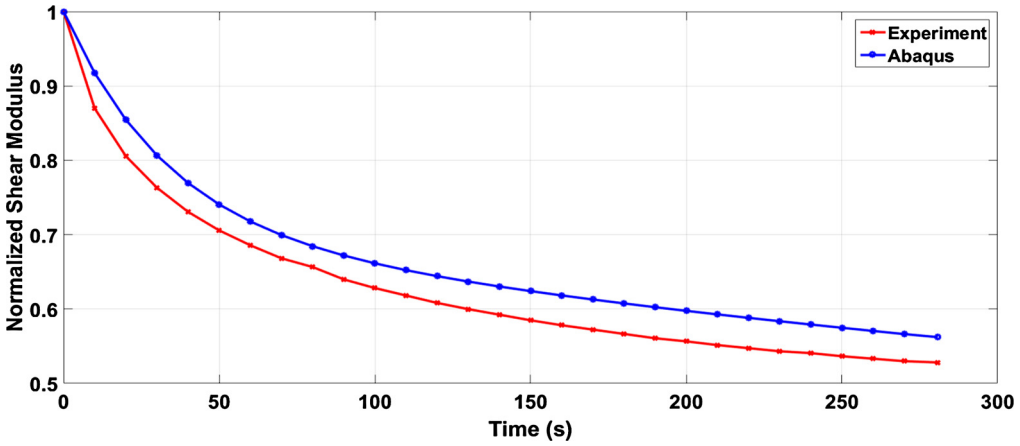

Fig. 8. Normalized shear modulus vs time.

Table 5
Prony series coefficients.

$G(i)$		$K(i)$	Tau(i)
1	0.2950	0	23.90
2	0.4050	0	451.61

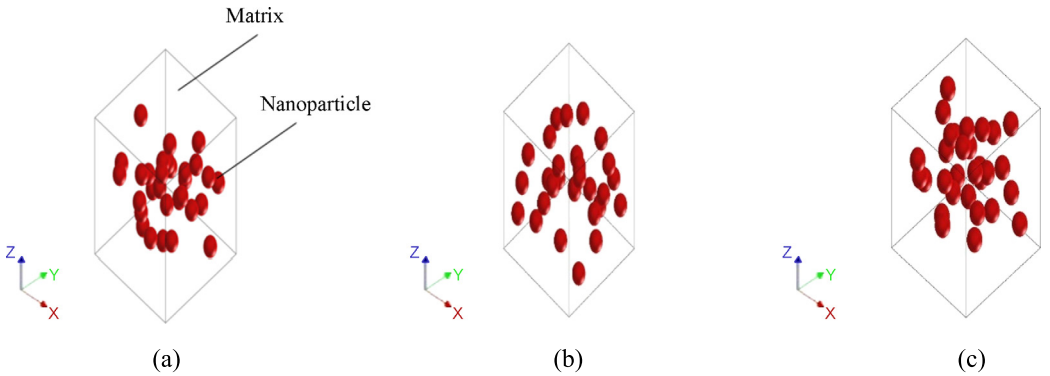

Fig. 9. (a) RVE showing the nanostructure for a filler concentration of 8%. (b) RVE showing the nanostructure for a filler concentration of 9%. (c) RVE showing the nanostructure for a filler concentration of 10%.

$$g_R(t) = 1 - \sum_{i=1}^{N} g_i^{-p}\left(1 - e^{\frac{-t}{\tau_i^G}}\right) \tag{2}$$

3.3. Finite-element modelling

The nanostructure of the silica-reinforced photopolymer matrix nanocomposite is shown by a 3D RVE (220 nm each side) for filler concentrations of 8%, 9%, and 10%, as shown in Fig. 9 (a, b, and c), respectively. Thirty similar spherical silica nanoparticles are randomly dispersed in the matrix. A random sequential adsorption algorithm [24] is used to generate nanoparticle centres, in which the probability of finding a nanoparticle at a given position is the same in all directions. The diameter of the nanoparticles depends on the volume fraction and the aspect ratio. An aspect ratio of 1 is chosen for all filler concentrations. As the silica nanoparticles have a diameter of about 30 nm, as shown in Fig. 3, the same value is used for a filler concentration of 8%, and the diameter increases with increasing the volume fraction. The elastic modulus of fumed silica nanoparticles was taken as $E_p = 70$ GPa and Poisson's ratio as $\nu_p = 0.3$. For the properties of epoxy/urethane matrix resin, calibrated Yeoh's hyperelastic material constants and Prony series coefficients were used as discussed in sections 3.1 and 3.2. Both phases are meshed with quadratic tetrahedron elements (C3D10M) with initial seed size of 11 nm, as shown in Fig. 10. In order to extend the RVE, periodic boundary conditions implemented from a user-defined python script were applied in all directions, i.e. by observing the interlinkage among the RVE and its reflecting images. A displacement vector **u** was used to express the periodic boundary conditions, which relates the displacement among the opposed ends to

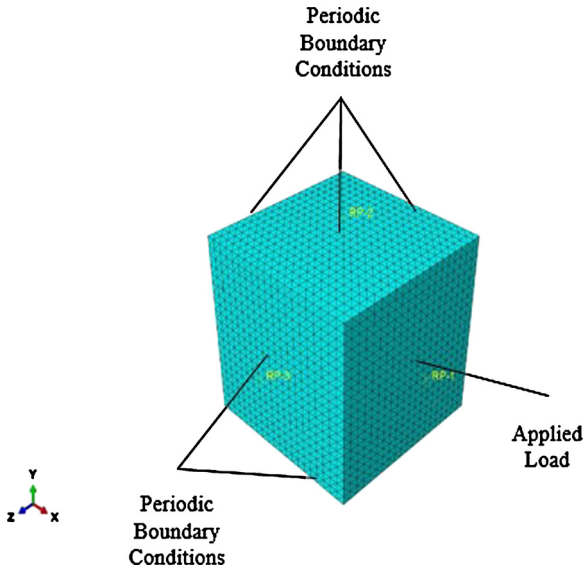

Fig. 10. RVE showing the periodic boundary conditions, the applied load, and the mesh.

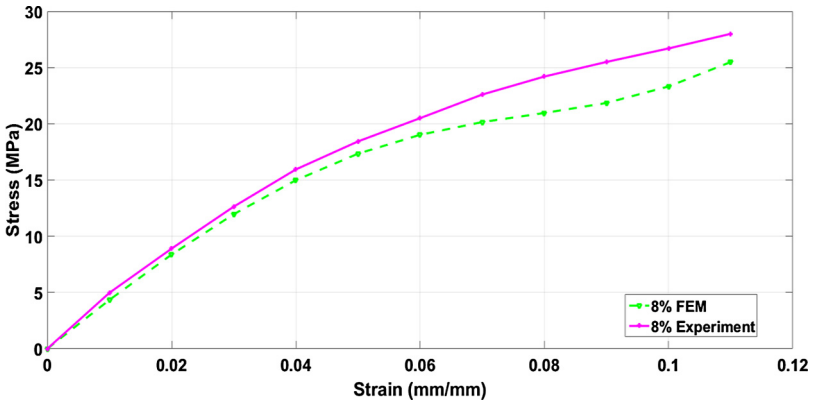

Fig. 11. Comparison of the stress–strain curves obtained from the experiments and the FEM for a filler concentration of 8%.

$$\boldsymbol{u}(x, y, 0) - \boldsymbol{u_z} = \boldsymbol{u}(x, y, L)$$
$$\boldsymbol{u}(x, 0, z) - \boldsymbol{u_y} = \boldsymbol{u}(x, L, z)$$
$$\boldsymbol{u}(0, y, z) - \boldsymbol{u_x} = \boldsymbol{u}(L, y, z)$$

in which L corresponds to the RVE length and x, y, and z are coordinate axes and $\boldsymbol{u_x}$, $\boldsymbol{u_y}$ and $\boldsymbol{u_z}$ **is** dependent on the load applied to the RVE. A strain equal to the strain at break observed during uniaxial tensile tests for each concentration was applied to the model in the x-direction.

3.4. FE simulations and model verification

A nanoscale RVE reinforced by silica filler with different concentrations was validated in this study, FE simulations were run on RVE composed of randomly dispersed nanoparticles with proper boundary conditions as discussed in section 3.3, and the results were compared with experiments. Many researchers have validated the hyperelastic models with experimental data [25–28] using different FE packages. In order to validate the proposed model, Yeoh's hyperelastic coefficients and Prony series coefficients were applied to the FE simulations of samples with filler concentrations of 8%, 9% and 10%; the results were compared with the tensile tests.

Figs. 12, 14, and 16 show the contour plots of the 8%, 9% and 10% filler concentrations, respectively. Figs. 12a, 14a, and 16a show the reaction forces of the respective filler concentrations; the stress was obtained by dividing the area of RVE with the reaction force. Figs. 12b, 14b, and 16b show the displacement of the respective filler concentration, strain was obtained by dividing the length of the RVE with displacement. Comparisons of the output obtained from the experiments and the FE model are depicted in Figs. 11, 13, 15. It is observed that the FE simulation with the hyper and viscoelastic

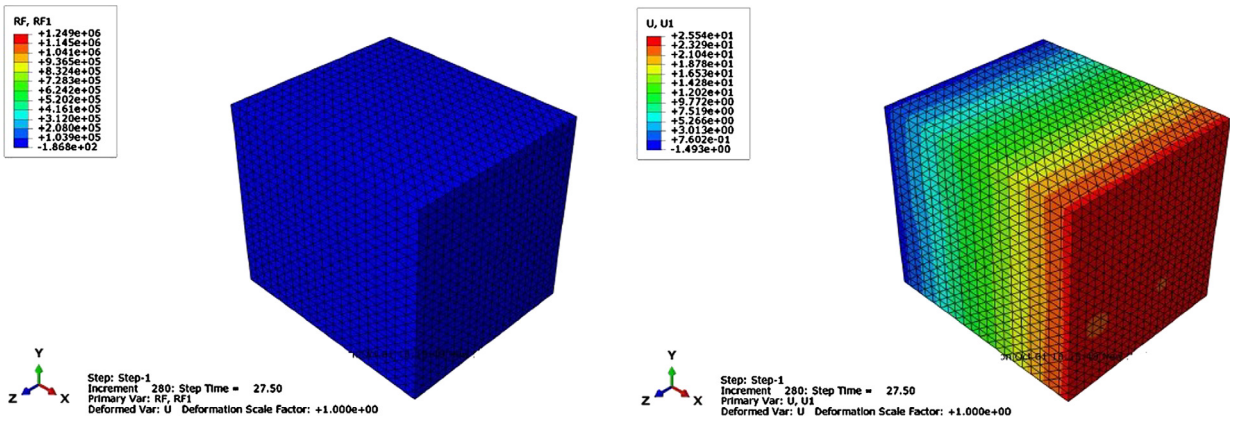

Fig. 12. Contour plot showing (a) the reaction force and (b) the displacement for a filler concentration of 8%.

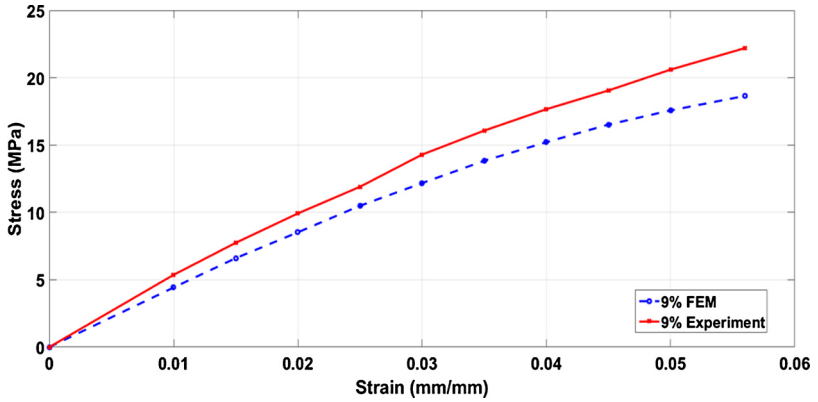

Fig. 13. Comparison of the stress–strain curves obtained from the experiments and the FEM for a filler concentration of 9%.

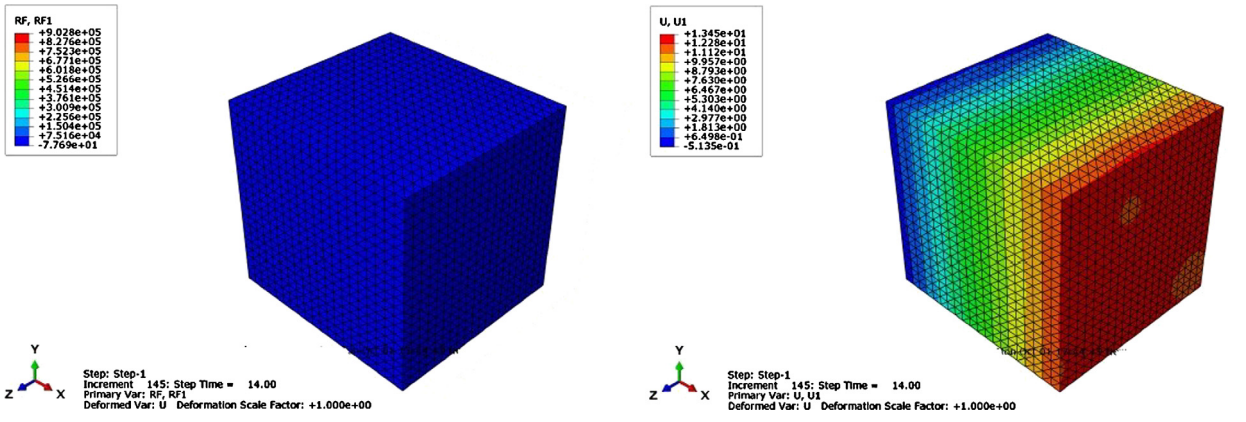

Fig. 14. Contour plot showing (a) the reaction force and (b) the displacement for a filler concentration of 9%.

models using Yeoh's SEDF is in good agreement with the experimental stress–strain curves of the samples printed with filler concentrations of 8%, 9%, and 10%.

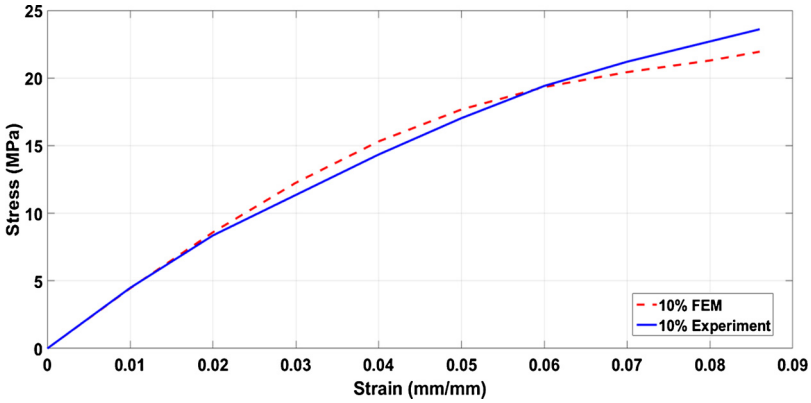

Fig. 15. Comparison of the stress–strain curves obtained from the experiments and the FEM for a filler concentration of 10%.

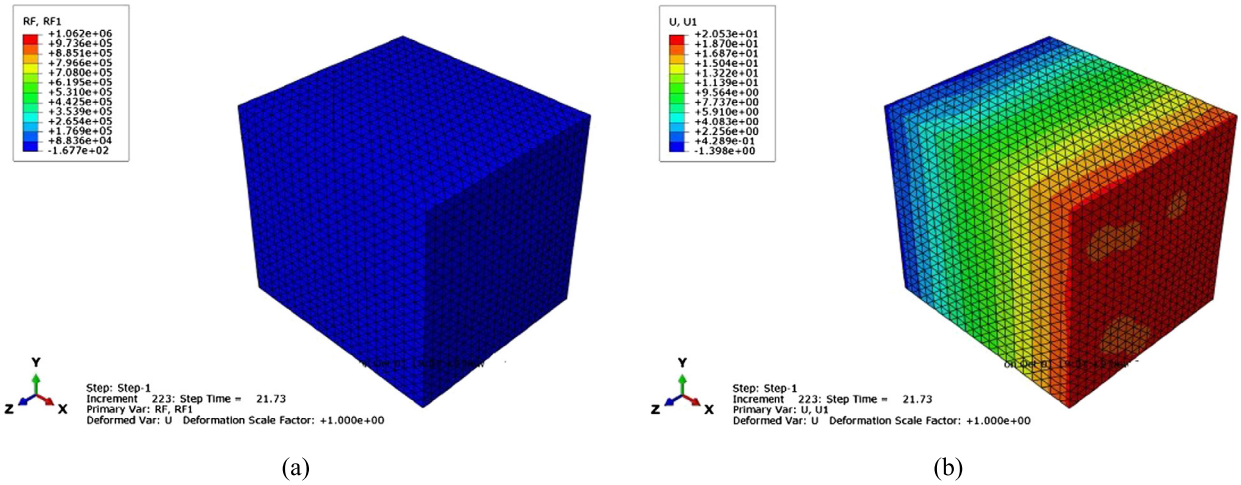

Fig. 16. Contour plot showing (a) the reaction force and (b) the displacement for a filler concentration of 10%.

4. Conclusion

In this paper, the mechanical properties of samples printed with a new 5-axis PPE printer have been studied. As this is a new technique and as the mechanical behaviour of the samples printed is yet to be explored, we have successfully carried out an experimental and numerical analysis of this new technique. The silica nano-filler is used as a reinforcement to enhance the mechanical properties of the photopolymer. Different concentrations of fumed silica filler have been added and its effect on mechanical properties have been analysed. A significant improvement in the tensile strength of the photopolymer is observed; for example, the tensile strength after the addition of 8%, 9% and 10% silica filler is 1.87, 1.48, and 1.57 times the tensile strength of the pure photopolymer, respectively. Although not demonstrated in this paper, but the new PPE printer is capable of printing free form and self-supported structures with its 5-axis printing capability. A finite-element model using hyper and viscoelastic phenomena has been developed and successfully corroborated with the experimental results. The multi-scale material modelling platform DIGIMAT was used to develop the RVE to represent the nanostructure of the nanocomposite; silica nanoparticles were randomly dispersed and proper boundary conditions were applied. The properties of the matrix were represented by Yeoh's material constant and Prony series coefficients. FE simulations were conducted using ABAQUS after importing the user-defined python script. The developed FE model based on hyper and viscoelastic phenomena successfully captured the behaviour of a silica-nanoparticle-reinforced photopolymer composite manufactured using a new 5-axis PPE printer. By employing the combination of hyperelasticity and viscoelasticity, the model is found to be in good agreement with the experimental stress–strain relationships for 8%, 9%, and 10% filler concentrations.

References

[1] Q. Zhang, M. Tian, Y. Wu, G. Lin, L. Zhang, Effect of particle size on the properties of Mg(OH)2-filled rubber composites, J. Appl. Polym. Sci. 94 (6) (2004) 2341–2346.
[2] A. Lazzeri, Y.S. Thio, R.E. Cohen, Volume strain measurements on CACO3/polypropylene particulate composites: the effect of particle size, J. Appl. Polym. Sci. 91 (2) (2004) 925–935.

[3] Y. Nakamura, M. Yamaguchi, M. Okubo, T. Matsumoto, Effect of particle size on mechanical properties of epoxy resin filled with angular-shaped silica, J. Appl. Polym. Sci. 44 (1) (1992) 151–158.
[4] X. Ling Ji, J. Kai Jing, W. Jiang, B. Zheng Jiang, Tensile modulus of polymer nanocomposites 42 (2002) 983–993.
[5] S. Mishra, S.H. Sonawane, R.P. Singh, Studies on characterization of nano $CaCO_3$ prepared by the in situ deposition technique and its application in PP-nano $CaCO_3$ composites, J. Polym. Sci., Part B, Polym. Phys. 43 (1) (2005) 107–113.
[6] D. Schmidt, D. Shah, E.P. Giannelis, New advances in polymer/layered silicate nanocomposites, Curr. Opin. Solid State Mater. Sci. 6 (3) (2002) 205–212.
[7] B. Wetzel, F. Haupert, M.Q. Zhang, Epoxy nanocomposites with high mechanical and tribological performance, Compos. Sci. Technol. 63 (14) (2003) 2055–2067.
[8] H. Wang, Y. Bai, S. Liu, J. Wu, C.P. Wong, Combined effects of silica filler and its interface in epoxy resin, Acta Mater. 50 (17) (2002) 4369–4377.
[9] V. Cannillo, F. Bondioli, L. Lusvarghi, M. Monia, M. Avella, M. Errico, M. Malinconico, Modeling of ceramic particles filled polymer–matrix nanocomposites 66 (2006) 1030–1037.
[10] Y.J. Liu, X.L. Chen, Evaluations of the effective material properties of carbon nanotube-based composites using a nanoscale representative volume element, Mech. Mater. 35 (1) (2003) 69–81.
[11] D.R. Katti, K.S. Katti, J.M. Sopp, M. Sarikaya, 3D finite element modeling of mechanical response in nacre-based hybrid nanocomposites, Comput. Theor. Polymer Sci. 11 (5) (2001) 397–404.
[12] X.Y. Wang, X. Wang, Numerical simulation for bending modulus of carbon nanotubes and some explanations for experiment, Composites, Part B, Eng. 35 (2) (2004) 79–86.
[13] Y. Wang, C. Sun, X. Sun, J. Hinkley, G.M. Odegard, T.S. Gates, 2-D nano-scale finite element analysis of a polymer field, Compos. Sci. Technol. 63 (11) (2003) 1581–1590.
[14] J. Zhang, Q. Ouyang, Q. Guo, Z. Li, G. Fan, Y. Su, L. Jiang, E.J. Lavernia, J.M. Schoenung, D. Zhang, 3D Microstructure-based finite element modeling of deformation and fracture of SiCp/Al composites, Compos. Sci. Technol. 123 (2016) 1–9.
[15] Y. Hua, L. Gu, H. Watanabe, Micromechanical analysis of nanoparticle-reinforced dental composites, Int. J. Eng. Sci. 69 (2013) 69–76.
[16] Y. Hua, L. Gu, S. Premaraj, X. Zhang, Role of interphase in the mechanical behavior of silica/epoxy resin nanocomposites, Materials 8 (6) (2015) 3519.
[17] R. Kaye, T. Goldstein, D. Zeltsman, D.A. Grande, L.P. Smith, Three dimensional printing: a review on the utility within medicine and otolaryngology, Int. J. Pediatr. Otorhinolaryngol. 89 (2016) 145–148.
[18] F. Rengier, A. Mehndiratta, H. von Tengg-Kobligk, C.M. Zechmann, R. Unterhinninghofen, H.U. Kauczor, F.L. Giesel, 3D printing based on imaging data: review of medical applications, Int. J. Comput. Assisted Radiol. Surg. 5 (4) (2010) 335–341.
[19] Digimat – muli-scale material modelling platform, Available from https://www.e-xstream.com/products/digimat/about-digimat.
[20] M. Asif, J.H. Lee, M.J. Lin-Yip, S. Chiang, A. Levaslot, T. Giffney, M. Ramezani, K.C. Aw, A new photopolymer extrusion 5-axis 3D printer, Addit. Manuf. 23 (2018) 355–361.
[21] Sonics and Materials Inc Ultrasonic Homogenizer, Available from https://www.sonics.com/.
[22] S.-Y. Fu, X.-Q. Feng, B. Lauke, Y.-W. Mai, Effects of particle size, particle/matrix interface adhesion and particle loading on mechanical properties of particulate–polymer composites, Composites, Part B, Eng. 39 (6) (2008) 933–961.
[23] P. Dittanet, R.A. Pearson, Effect of silica nanoparticle size on toughening mechanisms of filled epoxy, Polymer 53 (9) (2012) 1890–1905.
[24] B. Widom, Random sequential addition of hard spheres to a volume, J. Chem. Phys. 44 (10) (1966) 3888–3894.
[25] M. Sasso, G. Palmieri, G. Chiappini, D. Amodio, Characterization of hyperelastic rubber-like materials by biaxial and uniaxial stretching tests based on optical methods, Polym. Test. 27 (8) (2008) 995–1004.
[26] D.J. Charlton, J. Yang, K.K. Teh, A review of methods to characterize rubber elastic behavior for use in finite element analysis, Rubber Chem. Technol. 67 (3) (1994) 481–503.
[27] O.H. Yeoh, Some benchmark problems for FEA from torsional behavior of rubber, Rubber Chem. Technol. 76 (5) (2003) 1212–1227.
[28] C.V.R. Mohan, J. Ramanathan, S. Kumar, A.V.S.S.K.S. Gupta, Characterisation of materials used in flex bearings of large solid rocket motors, Def. Sci. J. 61 (3) (2011) 264–269.